Experimental and analytical investigation of micro-particle velocity domain and particle-wall interaction in microchannel

Mohammad Hassan Saidi[a], R. Razaghi[b,], Mohammad Zabetian[c]

[a]Center of Excellence in Energy Conversion (CEEC), School of Mechanical Engineering, Sharif University of Technology, P.O.BOX 11155-9567, Tehran, Iran

[b]Department of Mechanical and Aerospace Engineering, Garmsar Branch, Islamic Azad University, Garmsar, Iran

[c]Department of Mechanical Engineering, Tarbiat Modares University, Tehran, Iran

(Communicated by Abasalt Bodaghi)

Abstract

Micro-particles transportation in microfluidics devices is of interest for processing suspensions such as drug delivery, pharmaceutics, and food. Analytical and experimental studies have been conducted to investigate the velocity domain of micro-particles in Low-Reynolds-number Poiseuille flow in a rectangular microchannel. The results are compared with the existing methodologies such as Lattice-Boltzmann simulation and show good agreement. Compared with similar studies, the comparison between the experimental and analytical results provides broader insight into the effects of walls on the hydrodynamic behavior of micro-particles in microchannels. The comparative results show that the velocity domain of the dispersed phase is affected by the particles-fluid hydrodynamic coupling and particles-wall interactions. Also, particles slip velocities can be significant with the increase of particles sizes and proximity to nearby walls. Furthermore, the distance from the walls in which the particle-wall interaction is quite considerable is determined, which is about the order of particles diameter. Also, the number of particles observed near the bottom wall in all particle sizes was approximately 10% to 20% more than the number of particles found near the top wall, indicating the tendency of particles to sedimentation.

Keywords: Microchannel, Microparticles, Experimental Study, Analytical Solution, Particle-Wall Interaction
2020 MSC: 39B52, 39B72, 39B82, 47H10

1 Introduction

Microfluidics is an emerging field of technology that deals with the transport of particles in order of micrometers through minute volumes of fluid flowing in microchannels [25]. First research on microfluidics focused on single-phase flows [14]. However, many microfluidics applications are related to two-phase flows [27]. Two-phase flows contain a variety of categories based on the dispersed phase transported by the continuous phase [5], but the solid-liquid two-phase flow is being studied in the present research.

Many industrial and chemical applications are related to Particle transport in Low-Reynolds-number flows, such as flow cytometry, drug delivery, suspension processing, sedimentation, membrane separations, and blood flow analysis

[4]. The flow migration properties in such microflows are influenced by a variety of parameters such as Reynolds number, particle diameter-to-channel height ratio ($\frac{d_p}{H}$) and channel geometry, so that any study about the microfluidics applications should address the effects of mentioned factors on the hydrodynamic flow characteristics [8].

In solid-liquid microfluidics flows, most of the research focuses on methods of transporting fluid as a continuous phase containing particulate particles in various devices [26]. One of the earliest researches in the field of micro-particle hydrodynamics was presented by Lorentz [15] in which the motion of the particles near one plane wall at a small Reynolds number was studied. Furthermore, Jeffery [10] studied the rotation of a solid sphere with its axis of symmetry perpendicular to the plane. The solution of Jeffery was then expanded by Dean and O'Neil [6], who used spherical coordinates to derive the solution for a sphere rotating and translating in the vicinity of a plane wall about an arbitrary axis. The motion of a single particle between two flat planes was also considered by Faxen (2012). His solution focused on the migration of a spherical particle located at the centerline or at one-fourth of the distance between the two walls. Brenner [3] also performed a series of studies about the motion of a particle between two parallel walls migrating towards or away from walls.

Staben et al. [24] studied numerically the motion of a spherical particle between two parallel planes considering different effective parameters, including various particle sizes and particle–wall distances using boundary integral (B.I.) method. The results showed that the velocities of particles moving at the center region of the channel are about the same as the fluid and the slip velocities of particles increase at the regions near the channel walls. Similar work was conducted by Nikoubashman et al. [16] by performing Lattice-Boltzmann simulation to investigate the velocity domain of a single spherical particle migrating between two walls at different wall distances and achieved good agreement with Staben et al. [24].

You et al. [29] investigated the motion of micro-particles in the near-wall region using direct numerical simulation. Their results showed that the particles with Stokes number on the order of 0.1 gathered mostly in the region near the wall. Also, Silva [23] investigated numerically and experimentally the effect of the surface roughness on the behavior of the particles moving near the walls. The results showed that in the distances away from the walls, the experimental and numerical results were in good agreement, but near the walls, velocity magnitude derived from experiments was higher than the numerical ones due to the influence of particle surface roughness. The velocity domain and flow rate of the water flowing through a microchannel were determined by Puccetti et al. [18], Wang et al. [28] and Ashwood et al. [2] using the micro-PIV technique. Their results showed that micro-PIV is a suitable technique for the channels made by glass. Also, the experimental values of slip velocities of particles in the center of the channel have 1-4% differences with respect to theoretical ones. Furthermore, Khodaparast et al. [13] employed micro particle shadow velocimetry (μPSV) to measure dispersed particles' velocity domain in a rectangular microchannel. The results showed that using the mentioned approach would increase the reliability and accuracy of particle velocimetry. Alpers et al.[1] developed a dynamic discrete tomography algorithm for 3D particle tracking velocimetry. The results showed good agreement with the experiments.

Thermal effects on the particles moving through a mini-channel were examined experimentally [32] and theoretically [33] by Zabetian. The results showed that the induced flow caused by thermal effects was mainly due to the particles' thermophysical properties and absorption coefficient.

The velocity domain investigation of particles through the channels has the advantage of the determination of forces acting on the particles. The hydrodynamic forces acting on the particles in a laminar tube flow were determined by Eichhorn et al. [7] through an experimental technique. Also, the lift force on a particle moving through a rectangular channel in Poiseuille flow was investigated by Joseph et al. [11]. They found that particles tend to congregate at an equilibrium distance from the wall, called the "Sere' Silberberg" radius [21]. Zeng et al. [34] performed direct numerical simulations of a spherical particle translating parallel to a flat wall to obtain the lift force imposed on the particles. It was found that the lift coefficient decreases as both Reynolds number and distance from the wall increase.

According to the literature, microfluidics design, including microchannels, dispersed particles, and visualization techniques, depends on different parameters such as geometrical parameters, hydrodynamic conditions and fluid properties. In this paper, the analytical formulation introduced in [11] is employed thorough the proposed experimental setup to study the velocity field and slip velocity of the micro-particles in the microchannel and compared with experimental results. The testbed developed by the authors can measure the velocity field of the particles using the image processing technique. Differences between the proposed analytical model and experimental results in the velocity domain of particles are discussed. The distance from the walls in which the particles are strictly under the influence of walls is determined. Furthermore, the investigation can provide valuable data applicable for validation of numerical simulations of micro-size particulate flows.

2 Analytical Model

Figure 1 shows a circular particle of diameter d_p in a rectangular microchannel consisting of two parallel planes with a distance of H apart. The fluid and the particle are assumed to be density matched, so the buoyancy term does not enter into the model formulation.
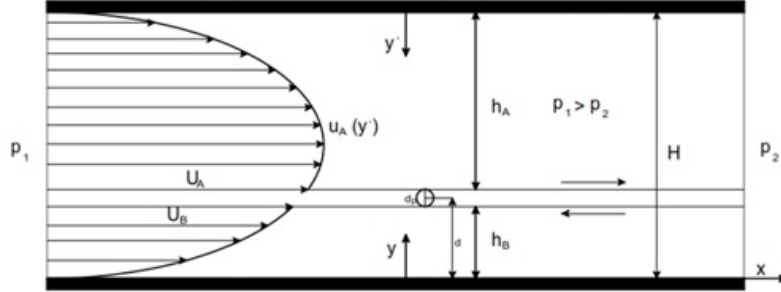

Figure 1: Schematic of flow field under consideration and variables involved in the model

The hydrodynamic forces acting on the particle stem from pressure force acting on the sides of the particle perpendicular to the flow and the shear stress force acting on the sides parallel to the flow [11]:

$$(\tau_A + \tau_B)l + (P_1 - P_2)d_p = 0 \tag{2.1}$$

$$\bar{P} = \frac{(P_1 - P_2)}{l}, \quad \tau_A + \tau_B + \bar{P}d_p = 0 \tag{2.2}$$

where, τ_A and τ_B are the shear stresses on the upper and lower side of the particle, P_1 and P_2 are the pressure acting on the left and right side of the particle and d_p and l are the diameter and length of the particle, respectively. The shear stresses are defined by:

$$\tau_A = -\eta \frac{du_A}{dy'}(h_A), \quad \tau_B = -\eta \frac{du_B}{dy}(h_B) \tag{2.3}$$

The velocity profiles above and below the particle can be written as:

$$\mathbb{A}^n_{(p_1,p_2,p_3)} := \{\mathfrak{A}_n \in \mathbb{A}^n | \text{ Card}\{A_j : A_j = x_{1j}\} = p_1,$$
$$\text{Card}\{A_j : A_j = x_{2j}\} = p_2, \text{Card}\{A_j : A_j = x_{1j} + x_{2j}\} = p_3, \}.$$

The following notations can be used for the multi-cubic mappings.

$$(\tau_A + \tau_B)l + (P_1 - P_2)d_p = 0 \tag{2.4}$$

and

$$u_B(y) = \frac{\bar{P}}{2\eta}y(h_B - y) + \frac{U_B y}{h_B} \tag{2.5}$$

where, U_A and U_B are assumed as velocities for the top and bottom of the particle to take into account the angular velocity of the circular particle, respectively. The difference between these two velocities is given by:

$$U_A - U_B = \frac{1}{2}\dot{\gamma}(h_B + \frac{1}{2}d_p)d_p \tag{2.6}$$

where, $\dot{\gamma}(y)$ is the shear rate for the undisturbed flow (particle-free fluid), given by:

$$\dot{\gamma}_{(y)} = \frac{du}{dy} = \frac{\bar{P}}{2\eta}(H - 2y) \tag{2.7}$$

he shear rate on the particle's sides may be evaluated from equations (2.4), (2.5) and (2.6):

$$\frac{du_A}{dy'}(h_A) = -\frac{\bar{P}}{2\eta}h_A + \frac{U_B}{h_A} + \frac{\dot{\gamma}(h_B + \frac{1}{2}d_p)}{2} \times \frac{d_p}{h_A} \tag{2.8}$$

$$\dot{\gamma}_{(y)} = \frac{du}{dy} = \frac{\bar{P}}{2\eta}(H - 2y) \tag{2.9}$$

Substituting equations (2.8) and (2.9) in Eq. (2.3), and then the resulting equation into Eq. (2.2), the velocity at the top and bottom of the particle can be found:

$$U_A = \frac{(\frac{\bar{P}}{\eta})(2d_p + h_A + h_B)h_A h_B + \dot{\gamma}(h_B + \frac{d_p}{2})h_A d_p}{2(h_A + h_B)} \tag{2.10}$$

$$U_A = \frac{(\frac{\bar{P}}{\eta})(2d_p + h_A + h_B)h_A h_B + \dot{\gamma}(h_B + \frac{d_p}{2})h_B d_p}{2(h_A + h_B)} \tag{2.11}$$

The average particle velocity is:

$$U_p = \frac{1}{2}(U_A + U_B) = \frac{(\frac{\bar{P}}{\eta})(2d_p + h_A + h_B)h_A h_B + \dot{\gamma}(h_B + \frac{d_p}{2})(h_B - h_A)\frac{1}{2}d_p}{2(h_A + h_B)} \tag{2.12}$$

The velocity profile of the undisturbed flow field can be written as:

$$u(y) = \frac{\bar{P}}{2\eta}y(H - y) \tag{2.13}$$

At a position where the center of the particle is located at $y_p = h_B + \frac{1}{2}d_p$, the undisturbed fluid velocity is:

$$u(h_B + \frac{1}{2}d_p) = \frac{\bar{P}}{2\eta}(h_B + \frac{1}{2}d_p)(h_A + \frac{1}{2}d_p) \tag{2.14}$$

The particle slip velocity can be defined as:

$$U_s = u(h_B + \frac{1}{2}d_p) - U_P \tag{2.15}$$

which can be written as:

$$U_s = \frac{(\frac{\bar{P}}{2\eta})[(h_A + h_B)(h_B + \frac{1}{2}d_p)(h_A + \frac{1}{2}d_p) - (2d + h_A + h_B)h_A h_B] + \dot{\gamma}(h_B + \frac{1}{2}d_p)(h_B - h_A)\frac{1}{2}d_p}{2(h_A + h_B)} \tag{2.16}$$

The above analytical formulations have been employed in order to calculate the slip velocity of three different particle sizes as 20 μm, 40 μm, and 60 μm migrating in the rectangular microchannel consisting of two parallel plates with the distance of 230 µm apart. The viscosity of the fluid has been considered similar to experiments as 0.0015 Pa.s, and the density of the particle and fluid was assumed to be equal to 1.05 $\frac{gr}{cm^3}$. Figure 2 shows the dimensionless slip velocity of three different particles with the ratio of diameter to channel height $\frac{d_p}{H}$ = 0.1, 0.2, and 0.3 versus the distance of the particle center from the lower wall, d, nondimensionalized by the channel height, H.
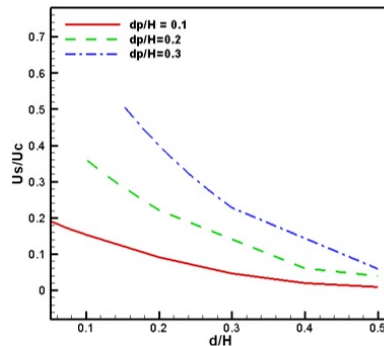

Figure 2:   Dimensionless slip velocity of particles versus dimensionless distance of particle center from the lower wall for three particle sizes with three diameter-to-channel height ratios

The particle diameter-to-channel height ratio, $\frac{d_p}{H}$, is an essential geometrical parameter for the transportation of micro-particles in microchannels. As it is clear from Fig. 2, with the increase of particle diameter, slip velocity of

particle increases as well. Furthermore, the differences between slip velocities of three particles in the middle of the channel are about 1-5%, exceeding almost 70% in the near-wall regions. Thus, the ratio of particle diameter to the channel height, $\frac{d_p}{H}$, is the parameter that affectsthe particle-fluid coupling and particle-wall interaction pronouncedly. For a particle migrating in a microchannel, there is a region in which the particle motion is affected quietly by the walls, and the slip velocity of the particle increases drastically due to particle-wall interaction. Out of this region, the hydrodynamic coupling has a significant role in the particles' drag force and slip velocity. Accordingly, understanding the wall-effect regions on the reduction of particle velocities could enhance the knowledge of experimental testbeds designated for micro-particle transportation in microchannels.

3   Experimental testbed

Figure 3 illustrates the schematic of the experimental setup, which contains three main parts: suspension characteristics, microchannel designation, and imaging system.
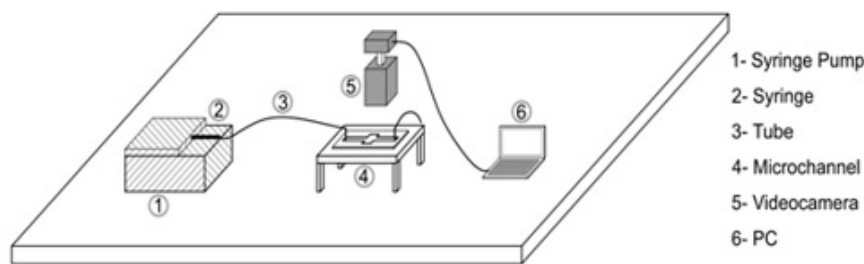

Figure 3: Schematic of the testbed

The driving force of the suspension through the microchannel is considered to be performed by a syringe pump, namely SP1000HOM from FNM Company [20]. The syringe pump volume rates range are 0.5 ± 0.005 $\mu liter/hr$ and 640 ± 0.015 ml/hr, respectively. A 1000 μliter glass syringe fabricated from ILS Company (Innovative Labor System GmbH, Germany) is connected to the syringe pump to inject the suspension through the channel with high accuracy. The suspension includes micro-particles ranging from 20-100 µm dispersed in the water-glycerol solution using an ultrasonic bath. The density of the solution is adjusted with the density of the particles, using pycnometer, so that the sedimentation is ignored in the measurements and calculations. Zabetain et al. [31, 32, 33] have comprehensively investigated the solvent properties. According to their studies, distilled water was selected as the primary phase. In order to match the density of continuous and dispersed phase, a solution of 19 percent glycerol by weight ($\rho_{gl} = 1.26\frac{g}{cm^3}$) in water was used to achieve a fluid density of $\rho_{sol} \cong 1.05 \pm 0.002 fracgcm^3$ at the room temperature of $22 \pm 1°C$. At this temperature, the water-glycerol solvent has a dynamic viscosity of $\mu = 0.0015 Pa.s$. with the accuracy of 10^{-5} [20].

The polished Soda Lime glass, which has stable chemical properties using the wet etching technique, is used to fabricate the rectangular microchannel [20]. The thickness of the glass used for fabricating the microchannel is a minimum 1 mm, so the movements of particles can be captured by the imaging system through the transparent and thin plate. The depth of the channel is 230 µm. The injection of the particulate flow is done through the inlet and outlet of the microchannel, which are made by two needles installed and sealed into two 1mm holes machined on the second glass and attached to the microchannel. The 2-D schematic of the microchannel is shown in Figure 4. All dimensions are in millimeters.
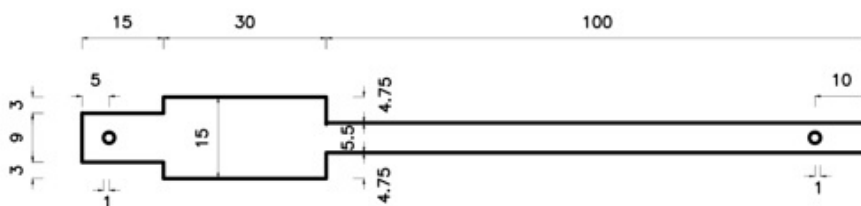

Figure 4: 2-D Plan of Fabricated Microchannel

An inverted microscope, along with a 2 Megapixels CCD camera, is used to visualize and record the migration of the particles. The domain of view is scaled with the scaling test slide. Each pixel of the images can be mounted as $0.52\,\mu m$ with a magnification of 20X for the objective. Table 1 shows the features of the imaging system.

Table 1: General Features of Imaging System

ine CCD FPS Range	25
ine Magnification of the Object	20X
ine No. of Pixels in Length	1280
ine No. of Pixels in width	1024
ine The domain of View (mm^2)	0.35
ine Spatial Resolution (μm)	0.52
ine	

4 Design of experiments

The syringe was filled with the prepared suspension and installed on the syringe pump at the first step. A 15 cm polystyrene tube was used to connect the needle of the syringe to the inlet of the microchannel. The particulate flow entirely filled the channel with the volume rate of 50 $\mu liter/min$. After that, the flow rate was set to $2.36 \pm 0.001\,\mu liter/min$, and consequently, the Reynolds number was 0.005 in the mentioned flow rate. Particle concentration in the suspension preparation was kept less than 0.25%, so particle-particle interaction would be ignorable. The main properties of particles used in this study are given in Table 2.

Table 2: Main properties of spherical particles used in this study

ine Size (μm)	$\frac{d_p}{H}$	Chemical Composition	Density (gr/cm^3)	Refractive Index ($25 \circ C$)
ine 20 ± 0.5	0.09			
39.7 ± 0.4	0.17	Poly–(styrene– co–divinylbenzene)	1.05 ± 0.001	1.59
51.7 ± 0.4	0.22			
76.8 ± 0.5	0.33			
ine				

The velocity domain of the dispersed particles was obtained through imaging techniques. A 2 Mega-pixel video camera captured the images of the particles mounted on the eyepiece of the LabomedTM TCM 400 inverted microscope. The experimental setup is shown in Figure 5.
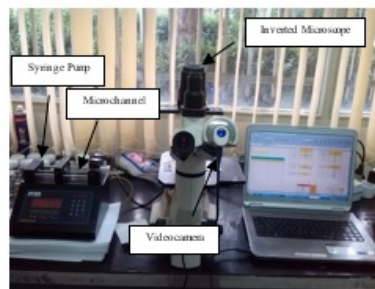

Figure 5: Experimental testbed

Particle images were recorded online with a computer connected to the videocamera within WinJoe Future software (Future Optics Sci., & Tech. Co., Ltd). A ruled glass micrometer was used in order to calibrate the motions of particles.

Each particle with a sharp and identified edge was labeled and tracked using image processing. By observing two consecutive images of a particle and connecting the centers of the particle, the displacement vector with the accuracy of one pixel can be obtained. These results were used to find the velocity domain of particles migrating through the microchannel.

Since all the particle velocities measurements were done by sweeping the channel height in different distances by microscopic imaging, the calibration of the microchannel was pivotal in results accuracy. To do so, the bottom and top walls of the channel were identified by rotating the coarse and fine knob of the microscope until the attached particles were observed clearly. After that, by dividing the rotation number of the knob by the channel height, every surface of the channel height would be determined. For LabomedTM TCM 400 inverted microscope, 230 degrees rotation of fine focus knob leads to swiping $230\ \mu m$ of the channel height. In order to determine the velocity domain of particles at the cross-section of the channel, the average velocity of particles migrating at the specific surface along the channel height should be calculated. To do so, the volume rate of the particulate flow was set to $2.36 \pm 0.001\ \mu liter/min$, and the microscope's field of view was fixed at the distance of $1.5\ cm$ from the channel entrance. At each surface of the channel height, particles in focus that had a sharp outline were identified and tracked for about 30-60 seconds. The velocity displacement vector of each particle was determined through the calibrated domain of view, and consequently, the average velocity of each particle was calculated by dividing the displacement magnitude by the time. Approximately 20 particles were observed for each surface of the channel height, and finally, the average particles' velocities were calculated at each level of the channel height, resulting in the velocity domain of the particles at the channel cross-section. Figure 6 shows a sample of the experiment in which the position and, consequently, the displacement vector of a particle was determined within 8 seconds of the flow. Similar steps have been fulfilled for approximately 20 particles in each level of the channel height, and finally, the average velocity of particles in each level was calculated.
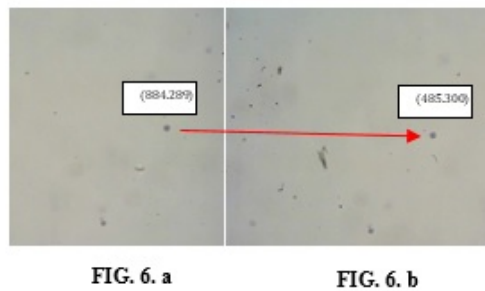

Figure 6: Determining the average particle velocity FIG. 6.a. Position of the particle in the second 72 of the start flow. FIG. 6.b. Position of the particle in the second 80 of the start flow

5 Results and Discussion

5.1 Pump Calibration

In this paper, all the velocities were non-dimensionalized by the centerline velocity, $\bar{U}_c$ The calibration of the syringe pump to produce a constant and reproducible flow was essential to obtain accurate results. All the experiments were performed at $Q = 2.36 \pm 0.001\ \frac{\mu liter}{min}$ which resulted in $Re = 0.005$. According to the calibrated domain of view, the uncertainty in the measurement of the location of the particle center was about 1 pixel or $0.52\mu m$ in x and y directions, leading to particle velocity measurement uncertainty of about 1-2%. Table 3 shows the results from the set of experiments and assures us that the syringe pump provides a constant and reproducible flow in the range of acceptable uncertainties. For particles with an average diameter of $20 \pm 0.5\ \mu m$, the magnitude of $\bar{U}_c$ was measured for five consecutive one-minute intervals at three different experiments at $Q = 2.36 \pm 0.001\ \frac{\mu liter}{min}$. All data were measured after 30 seconds of startup. Each value in Table 3 represents the average centerline velocity measurement of about 4-8 particles.

The small variations in the values of $\bar{U}_c$ may be due to eye error in determining the center of some particles away from the centerline of the channel height. However, all values have a maximum 10% difference from the average of experimental results in each experiment. So, it can be concluded that the values of Table 3 show that the syringe pump is calibrated and the flow is reproducible through the tests, and the velocity domain measurements data of the particles are valid.

Table 3: Pump calibration experiments for average centerline velocity at $Q = 2.36 \pm 0.001 \frac{\mu liter}{min}$

ine Intervals	$\bar{U}_c(\frac{\mu m}{s})$		
	Experiment #1	Experiment #2	Experiment #3
ine $0.5 - 1\, min$	39.65 ± 0.55	42.8 ± 0.79	44.06 ± 1.12
$1 - 2\, min$	43.9 ± 0.78	43.47 ± 1.78	42.98 ± 0.87
$2 - 3\, min$	44.45 ± 1.25	44.90 ± 0.41	41.43 ± 1.24
$3 - 4\, min$	41.34 ± 1.45	43.56 ± 0.57	40.12 ± 2.5
$4 - 5\, min$	42.89 ± 0.97	40.21 ± 2.3	43.24 ± 2.33
$0.5 - 5\, min$ (average)	42.45 ± 1.00	42.98 ± 1.17	42.37 ± 1.61
ine			

5.2   Particle velocity measurements

As discussed in section 2, the slip velocity between the particle and the fluid is influenced by two main factors: particle-fluid and particle-wall interaction. This can be quite noticeable when the particle migrates near the walls regions. In this part of the paper, this phenomenon is analytically and experimentally investigated.

Since, the ratio of particle diameter to the channel height, $\frac{d_p}{H}$, is one of the essential geometrical parameters in the transportation of micro-particles in microchannels, the formulations of the analytical model discussed in section 2 have been employed for three different particle sizes as $\frac{d_p}{H} = 0.1$ 0.2 and 0.3 to determine the velocity domain of the particles. The viscosity of the fluid was considered similar to the experiments as 0.0015 Pa.s and particles and fluid were assumed to be density matched as $1.05 \frac{gr}{cm^3}$. Based on the mentioned assumptions, the velocity fields of three different particles sizes were calculated and compared with experimental and numerical results. The particle velocity was calculated analytically for the half of the channel and mirrored for the rest of the channel cross-section based on the symmetry of the parabolic velocity profile. In the following results, H is the channel height, d is the distance of particle center from the lower wall, d_p is the particle diameter, a is the radius of the particle, and U_c is the centerline velocity of the particle-free flow. Figures 7 through 9 show the comparison of measured particle velocities (u), nondimensionalized by the average centerline velocity, U_c, versus the distance of particle center from the walls, d, scaled by the channel height, H. The solid curve is the particle-free Poiseuille flow velocity calculated by using a 3D computational fluid dynamics solution of fully-developed Poiseuille flow in a rectangular channel, and dashed curves are the Lattice-Boltzmann simulation results for $\frac{d_p}{H} = 0.1$ 0.2 and 0.3 from Nikoubashman et al. [16].

Figure 7 compares the velocity domain of $20 \pm 0.5\,\mu m$ particles in experiments with the velocity domain of particles with the ratio of $\frac{d_p}{H} = 0.1$ from the analytical solutions and Lattice-Boltzmann simulation. Good agreement between the experiments and the Lattice-Boltzmann simulation is shown in this figure. The experimental results for the velocity domain of $20 \pm 0.5\,\mu m$ particles show that, at the middle range of the channel, the maximum difference between the average velocities of particles with Lattice-Boltzmann simulations is about 2% and 5% near the walls. More differences between experiments and numerical results near the wall are due to particles attached to the walls, which affect the velocity domain of migrating particles. This phenomenon is neglected in the assumptions of the simulation.

Comparing the experimental and analytical velocity measurements shows good agreement in the middle regions of the channel. In the near-wall regions, analytical results show more velocity reduction than experiments. This deviation increases with the proximity of particles to the wall. This is since the particle-wall interaction source term has not been employed in the analytical formulations; thus, near-wall regions velocities of the analytical solution seem to have more differences from the experimental results. In other words, there is a distance near the wall in which the particle-wall interaction is quite significant. In this region, the experimental investigations release more reliable results than analytical ones. Table 4 compares average particle velocities of numerical and analytical studies.

The distance of wall-effect on the particles is significant for the designation of experimental testbeds in order to transport the specified number of particles through microchannels. Table 4 shows that in the middle of the channel,
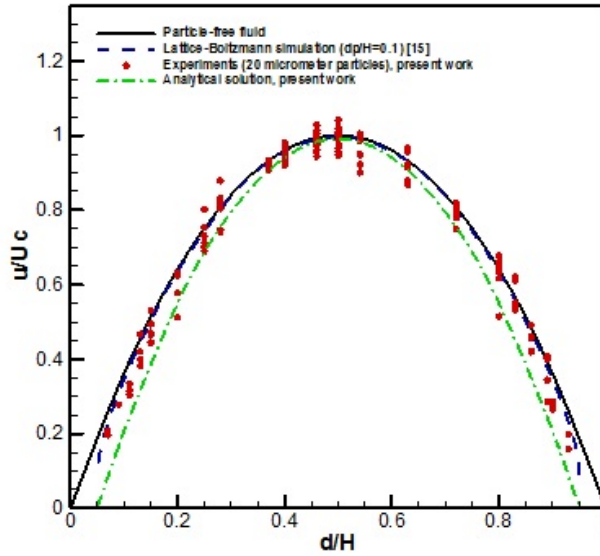
Figure 7: Experimental and analytical measurements of the particle velocity, $\frac{u}{U_c}$, vs. distance of particle center from the bottom wall, $\frac{d}{H}$, for 20 μm diameter particles ($\frac{d_p}{H} = 0.1$).

Table 4: Differences between the analytical and numerical velocity of particles with $\frac{d_p}{H} = 0.1$

ine $\frac{d}{a}$	$d(\mu m)$	analytical solution ($\frac{u}{U_c}$)	Lattice-Boltzmann[15] ($\frac{u}{U_c}$)	differences (%)
ine 0.5 $\frac{H}{a}$	100	0.991	0.997	0.5
ine 8	80	0.941	0.957	1.7
ine 6	50	0.794	0.836	4.9
ine 4	40	0.549	0.635	13.4
ine 2	20	0.208	0.345	39.8
ine 1.8	18	0.168	0.310	45.7
ine 1.6	16	0.128	0.272	53.1
ine 1.4	14	0.860	0.231	62.7
ine 1.2	12	0.043	0.183	76.2
ine 1.02	10.2	0.004	0.111	96.0
ine				

the difference between the Lattice-Boltzmann simulation and analytical solution is a minimum 0.5% and increases slightly with the decrease of particle distance to the wall until the particle center is located at 20 μm from the lower wall. After that, differences increase drastically up to 96% at 0.2 μm separations of particle and wall. In other words, the distance 20 μm from the wall is the distance in which the particle-interaction is significant, and wall effects on the particles increase pronouncedly. That is the reason the analytical solution is not capable of predictingwhy the analytical solution cannot predict the velocity of particles as with the same accuracy as experimental or numerical methods. ButHowever, outside of this region analytical solution could be a good substitution of expensive methods of experiment, analytical solution could be a good substitution for expensive experiments methods.

Figure 8 compares the velocity domain of $39.7 \pm 0.4 \, \mu m$ particles measured by experiments with the velocity domain of particles with the ratio of $\frac{d_p}{H} = 0.2$ from the analytical solutions and Lattice-Boltzmann simulation. Good agreement was achieved between experimental and numerical results. Compared with Figure 7, the difference between the experimental and numerical velocity domain lies at 1-2% in the middle regions of the channel and increases up to
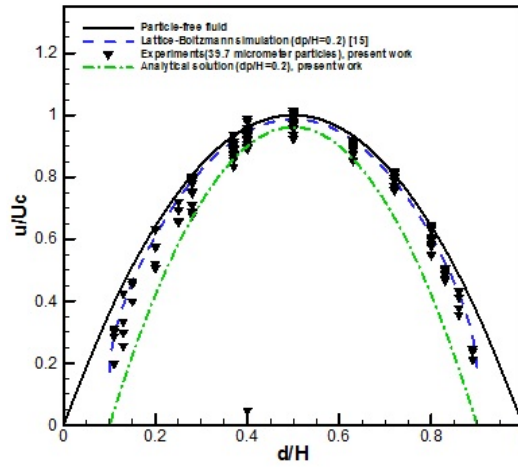
4-6% in near-wall regions.

Figure 8: Experimental and analytical measurements of the particle velocity, $\frac{u}{U_c}$, vs. distance of particle center from the bottom wall, $\frac{d}{H}$, for 39.7 μm diameter particles ($\frac{d_p}{H} = 0.2$).

Table 5 shows the comparison between average particles velocities of numerical and analytical study for $\frac{d_p}{H} = 0.2$. As mentioned before, the analytical solution has been done for half of the channel and extended to the rest of the channel section. Accordingly, no data is found for distances $d = 160\,\mu m$ and $d = 120\,\mu m$ in Table 5. Compared with the velocity domain of Table 4, the difference between the analytical and numerical velocity calculations exceeds to 2.6% in the middle of the channel and increases drastically to 31.1% in the distance 40 μm from the bottom wall and continues to almost 95% in the 4 μm separation of particle and the wall. Thus, it is worth mentioning that the distance near the wall in which the slip velocity of particles with 39.7 μm diameter increases significantly is 40 μm from the wall.

Table 5: Differences between the analytical and numerical velocity of particles with $\frac{d_p}{H} = 0.2$

ine $\frac{d}{a}$	$d(\mu m)$	analytical solution ($\frac{u}{U_c}$)	Lattice-Boltzmann[15] ($\frac{u}{U_c}$)	differences (%)
ine 0.5 $\frac{H}{a}$	100	0.961	0.987	2.6
ine 8	160	-	-	-
ine 6	120	-	-	-
ine 4	80	0.899	0.946	4.9
ine 2	40	0.420	0.61	31.1
ine 1.8	36	0.346	0.555	37.7
ine 1.6	32	0.266	0.494	46.1
ine 1.4	28	0.182	0.425	57.0
ine 1.2	24	0.094	0.342	72.6
ine 1.02	20.4	0.0096	0.209	95.4
ine				

Figure 9 compares the velocity domain of 76.8$\pm$0.5 μm particles measured by experiments with the velocity domain of particles with the ratio of $\frac{d_p}{H} = 0.3$ from the analytical solutions and Lattice-Boltzmann simulation. Compared with Figures 7 and 8, maximum slip velocity occurs in this range of particle sizes. Also, the maximum difference between the experiments and numerical results occurs close to the walls through this type of particle compared to other particle sizes. This may be due to the effect of particles attached to the walls, which is neglected in the simulations assumption.

Also, the maximum difference between the average velocities of 76.8 μm particles with the numerical results shows that the settling phenomenon in the velocity field of larger particles plays a more significant role than the smaller ones. Finally, the total number of particles observed near the bottom regions of the channel is about 20% more than the upper regions of the channel.
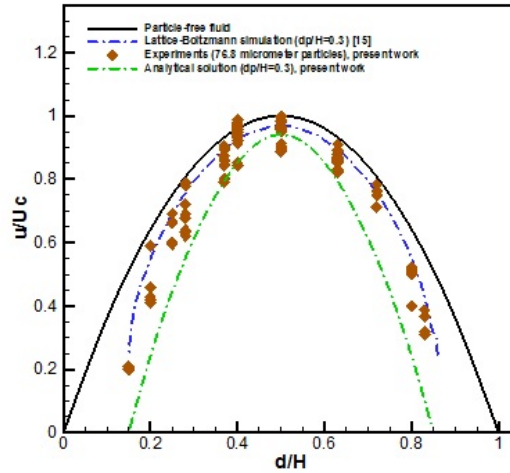

Figure 9: Experimental and analytical measurements of the particle velocity, $\frac{u}{U_c}$, vs. distance of particle center from the bottom wall, $\frac{d}{H}$, for 76.8 μm diameter particles ($\frac{d_p}{H} = 0.3$).

Table 6: Differences between the analytical and numerical velocity of particles with $\frac{d_p}{H} = 0.3$

ine $\frac{d}{a}$	$d(\mu m)$	analytical solution ($\frac{u}{U_c}$)	Lattice-Boltzmann[15] ($\frac{u}{U_c}$)	differences (%)
ine 0.5 $\frac{H}{a}$	100	0.941	0.970	2.9
ine 8	240	-	-	-
ine 6	180	-	-	-
ine 4	120	-	-	-
ine 2	60	0.613	0.796	23.0
ine 1.8	54	0.517	0.737	29.8
ine 1.6	48	0.408	0.668	38.9
ine 1.4	42	0.285	0.584	51.1
ine 1.2	36	0.149	0.476	68.6
ine 1.02	30.6	0.016	0.297	94.7
ine				

According to the results of Table 6, the difference between the analytical and numerical velocity domain in the middle of the channel for particles with $\frac{d_p}{H} = 0.3$ is about 3% and increases to 23% in the distance of 60 μm from the wall. Comparing with Tables 4 and 5, as the particle size increases the distance of wall-effect increases either. In other words, larger particles seem to be more affected by the walls than the smaller ones.

5.3 Wall-effect region of the channel

According to the results of Tables 4, 5 and 6, for a particle with 20 μm diameter, the differences between the analytical and numerical particle velocity measurements start to increase significantly when the particle is located at 20 μm from the lower wall. Similarly, for the particles with 39.7 μm and 76.8 μm diameters, this phenomenon

occurs when the particles are located at almost 40 μm and 60 μm from the lower wall. The differences between the analytical solution and experimental or numerical methods are that particle-wall interaction is not properly modelled in the analytical formulations. This is due to some simplifying assumptions in analytical relations in which the lateral migration of particle is being neglected, and the particle is assumed to move in the x-direction. However, in the wall-effect region of the channel, there is a lift force, namely, Saffman lift force, which acts on the particle and makes the particle to move in y-direction due to the high shear rate. Accordingly, it can be concluded that the wall-effect region of the channel is the distance in the vicinity of the walls in which the differences between the analytical velocity measurement with the experimental or numerical results grow significantly. This distance is determined as the order of the particle diameter. Moreover, when the particle moves in the distance of particle diameter from the walls, the particle-wall interaction dominates the particle-fluid hydrodynamic coupling, and the velocity domain of the particle should be calculated according to the particle-wall interaction consideration. Furthermore, particle-wall interaction increases with the proximity of the particle to the walls.

6   Conclusion

In this paper, an experimental setup based on image processing of micro-particles was introduced mainly due to investigate the velocity domain of particles with particle diameter-to-channel height ratio ranging from 0.1 to 0.3 ($0.1 \leq \frac{d_p}{H} \leq 0.3$) in a dilute suspension in low Reynolds number Poiseuille flow in a rectangular microchannel. This research aims to address an effective technique to consider particle tracking of micro-particles in microchannels. Furthermore, comparing the experimental data with the analytical results presented some deviations in the velocity domain of particles, particularly near the walls, which was neglected in the analytical formulations. The results show that the slip velocity of particles which is due to the difference between the velocity of particles and fluid, is minimum at the center of the channel and increases in the vicinity of walls. Furthermore, an increase in particles sizes leads to a decrease in particles velocities at the same particle center location due to the interaction effects of nearby walls.

Additionally, based on experimental observations, the number of particles observed near the bottom wall in all particle sizes was approximately 10% to 20% more than the number of particles found near the top wall, indicating the tendency of particles to settle down toward the bottom wall. Also, the difference between the average velocity of particles in the experimental and the numerical results in the middle area of the channel was observed to be 2% to 5% but near the walls was 4% to 10%. The smallest difference was related to particles with the diameter of $20 \pm 0.5\,\mu m$ and the highest difference occurred in the particles with the diameter of $76.8 \pm 0.5\,\mu m$ which is probably due to the effects of particles adhering to the walls in the experiments and is usually neglected in the numerical modeling assumptions.

The simplified analytical solution can predict the particle velocity domain outside the particle-affecting region and can be a good substitution by the expensive experimental methods. However, in the particle-wall effect regions in which the particle-wall interaction grows pronouncedly, the proposed method should be modified by the source term in which the particle-wall interaction is implemented adequately.

According to the comparative study between the experimental and analytical particle velocity measurements, the wall-effect region in the vicinity of the walls is the distance on the order of particle diameter. In other words, when the particle moves a distance in the order of particle diameter from the walls, the particle-wall interaction dominates the particle-fluid hydrodynamic coupling, and the velocity domain of the particle should be calculated according to the particle-wall interaction consideration. Furthermore, particle-wall interaction increases with the proximity of the particle to the walls. The proposed simplified analytical model fails to predict the velocity domain of the particles near the walls. So, further investigations might be necessary to develop the proper source term adding to the formulations for better agreement with the experimental results.

Acknowledgements

References

[1] A. Alpers, P. Gritzmann, D. Moseev, and M. Salewski, *3D particle tracking velocimetry using dynamic discrete tomography*, Comput. Phys. Commun. **187** (2015), 130–136.

[2] A. Ashwood, A.C. Ashwood, S.V. Hogen, M.A. Rodarte, C.R. Kopplin, D.J. Rodríguez, E.T. Hurlburt, and T.A. Shedd, *A multiphase, micro-scale PIV measurement technique for liquid film velocity measurements in annular two-phase flow*, Int. J. Multiphase Flow **68** (2015), no. 18, 27–39.

[3] H. Brenner, *The slow motion of a sphere through a viscous fluid towards a plane surface*, Chem. Engin. Sci. **16** (1961), no. 3, 242–251.

[4] R. Cox and S. Mason, *Suspended particles in fluid flow through tubes*, Ann. Rev. Fluid Mech. **3** (1971), no. 1, 291–316.

[5] E. Dario, L. Tadrist, and J. Passos, *Review on two-phase flow distribution in parallel channels with macro and micro hydraulic diameters: main results, analyses, trends*, Appl. Thermal Engin. **59** (2013), no. 1, 316–335.

[6] W. Dean and M. O'Neill, *A slow motion of viscous liquid caused by the rotation of a solid sphere*, Mathematika **10** (1963), no. 3, 13–24.

[7] R. Eichhorn and S. Small, *Experiments on the lift and drag of spheres suspended in a Poiseuille flow*, J. Fluid Mech. **20** (1964), no. 3, 513–527.

[8] P. Gravesen, J. Branebjerg, and O.S. Jensen, *Microfluidics-a review*, J. Micromech. Microengin. **3** (1993), no. 4, 168.

[9] J. Happel and H. Brenner, *Low Reynolds Number Hydrodynamics: With Special Applications to Particulate Media*, Springer Science & Business Media, 2021.

[10] G. Jeffery, *On the steady rotation of a solid of revolution in a viscous fluid*, Proc. London Math. Soc. **2** (1915), no. 1, 327–338.

[11] D. Joseph and D. Ocando, *Slip velocity and lift*, J. Fluid Mech. **454** (2002), 263–286.

[12] H. Keramati, M. Saidi, and M. Zabetian, *Stabilization of the suspension of Zirconia microparticle using the nanoparticle Halos mechanism: Zeta potential effect*, J. Dispersion Sci. Technol. **37** (2015), no. 1, 6–13.

[13] S. Khodaparast, N. Borhani, and J. Thome, *Application of micro particle shadow velocimetry PSV to two-phase flows in microchannels*, Int. J. Multiphase Flow **62** (2014), 123–133.

[14] Y.W. Kim and J.Y. Yoo, *Transport of solid particles in microfluidic channels*, Optics Lasers Engin. **50** (2012), no. 1, 87–98.

[15] H. Lorentz, *A general theorem concerning the motion of a viscous fluid and a few consequences derived from it*, Zittingsverlag Akad. Wet. Amsterdam **5** (1986), 168–75.

[16] A. Nikoubashman, C.N. Likos, and G. Kahl, *Computer simulations of colloidal particles under flow in microfluidic channels*, Soft Matter **9** (2013), no. 9, 2603–2613.

[17] M. O'neill, *A slow motion of viscous liquid caused by a slowly moving solid sphere*, Mathematika **11** (1964), no. 1, 67–74.

[18] G. Puccetti, B. Pulvirenti, and G.L. Morini, *Experimental determination of the 2D velocity Laminar profile in glass microchannels using*, PIV, Energy Procedia **45** (2014), 538–547.

[19] R. Razaghi and M.H. Saidi, *Transportation and settling distribution of microparticles in low-reynolds-number poiseuille flow in microchannel*, J. Dispersion Sci. Technol. **37** (2016), no. 4, 582–594.

[20] R. Razaghi and M.H. Saidi, Mohammad Hassan, *Experimental investigation of drag and lift forces on micropar-ticles in low Reynolds number poiseuille flow in microchannel,* J. Dispersion Sci. Technol. **37** (2016), no. 12, 1767–1777.

[21] R. Razaghi, F. Shirinzadeh, M. Zabetian, and E. Aghanoorian, *Velocity domain and volume fraction distribution of heavy microparticles in low Reynolds number flow in microchannel*, J. Dispersion Sci. Technol. **38** (2017), no. 3, 374–380.

[22] G. Segre and A. Silberberg, *Radial particle displacements in Poiseuille flow of suspensions*, Nature **189** (1961), no. 4760, 209-210.

[23] G. Silva, N. Leal, and V. Semiao, *Micro-PIV and CFD characterization of flows in a microchannel: velocity*

profiles, surface roughness and Poiseuille numbers, Int. J. Heat Fluid Flow **29** (2008), no. 4, 1211–1220.

[24] M.E. Staben, A.Z. Zinchenko, and R.H. Davis, *Motion of a particle between two parallel plane walls in low-Reynolds-number Poiseuille flow*, Phys. Fluids (1994-present), **15** (2003), no. 6, 1711–1733.

[25] P. Tabeling, *Introduction to Microfluidics*, Oxford University Press, 2010.

[26] A. Terray, J. Oakey, and D.W. Marr, *Microfluidic control using colloidal devices,* Science **296** (2002), no. 5574, 1841–1844.

[27] A.M.C. Van Dinther, C. Schroën, F.J. Vergeldt, R.G.M. Van der Sman, and R.M. Boom, *Suspension flow in microfluidic devices—A review of experimental techniques focussing on concentration and velocity gradients*, Adv. Colloid Interface Sci. **173** (2012), 23–34.

[28] H. Wang and Y. Wang, *Measurement of water flow rate in microchannels based on the microfluidic particle image velocimetry*, Measurement **42** (2009), no. 1, 119–126.

[29] C. You, C.F. You, G.H. Li, H.Y. Qi, and X.C. Xu, *Motion of micro-particles in channel flow*, Atmosph. Envir. **38** (2004), no. 11, 1559–1565.

[30] M. Zabetian, M.H. Saidi, M.S. Saidi, and M.B. Shafii, *Thermal interaction of laser beam with particulate flow in mini-channels*, ASME 2011 9th Int. Conf. Nanochan. Microchan. Minichan., American Society of Mechanical Engineers, 2011.

[31] M. Zabetian, M.H. Saidi, M.S. Saidi, and M.B. Shafii, *Modeling of laser thermal and hydrodynamic effects on a dilute suspension of micro-particles in water*, J. Mech. Sci. Technol. **28** (2014), no. 3, 1017–1026.

[32] M. Zabetian, M.S. Saidi, M.B. Shaffi, and M.H. Saidi, *Separation of microparticles suspended in a minichannel using laser radiation pressure*, Appl. Optics **52** (2013), no. 20, 4950–4958.

[33] M. Zabetian, M.B. Shaffi, M.H. Saidi, and M.S. Saidi, *A new experimental approach to investigate the induced force and velocity fields on a particulate manipulation mechanism*, Sci. Iran. Trans. B, Mech. Engin. **21** (2014), no. 2, 414.

[34] L. Zeng, S. Balachandar, and P. Fischer, *Wall-induced forces on a rigid sphere at finite Reynolds number*, J. Fluid Mech. **536** (2005), 1.